Complete fusion of $^{74}Ge + ^{74}Ge$

M. Beckerman, M. K. Salomaa, J. Wiggins, and R. Rohe
Laboratory for Nuclear Science, Massachusetts Institute of Technology, Cambridge, Massachusetts 02139
(Received 14 June 1983)

Differential cross sections for evaporation residue formation following complete fusion of ^{74}Ge with 218–305 MeV ^{74}Ge ions were measured with high precision using a velocity selector together with a counter telescope. The resulting excitation function for complete fusion ranged in magnitude from 435 mb near 150 MeV down to 27 μb at 108.5 MeV (c.m.). We observed increases in the sub-barrier fusion of $^{74}Ge + ^{74}Ge$, compared to $^{58,64}Ni + ^{74}Ge$, consistent with those observed previously in systems where ^{74}Ge replaces either ^{58}Ni or ^{64}Ni as a collision partner. Correlations between variations among fusion excitation functions for the $^{58}Ni + ^{58}Ni$ to $^{74}Ge + ^{74}Ge$ systems and the underlying nuclear structure were examined. We discussed nucleon transfer and other dynamic processes which may be responsible for the complex variations and for the overall increases in sub-barrier fusion observed in comparisons to static, barrier penetration calculations.

[NUCLEAR REACTIONS Complete fusion, $^{74}Ge + ^{74}Ge$ $E = 218$–305 MeV (lab), measured $\sigma(E,\theta)$ for evaporation residues; discussed fusion dynamics.]

I. INTRODUCTION

In this paper we present results of measurements of cross sections for evaporation residue formation following complete fusion of $^{74}Ge + ^{74}Ge$. These experiments complete the cycle of measurements of excitation functions for complete fusion of ^{58}Ni, ^{64}Ni, and ^{74}Ge with one another from near-to-far sub-barrier energies. The experiments were motivated by the observation that it is at sub-barrier energies, where the detailed dynamics are not masked by pocket trapping, that one may probe the early stages of the fusion process and its interplay with the underlying nuclear structure.

In our previous studies,[1–3] we investigated the $^{58}Ni + ^{58}Ni$, $^{58}Ni + ^{64}Ni$, $^{64}Ni + ^{64}Ni$, $^{58}Ni + ^{74}Ge$, and $^{64}Ni + ^{74}Ge$ systems. We found that the far sub-barrier cross sections varied from system to system by several orders of magnitude beyond that which could be ascribed to barrier height/position differences. Of the five systems studied, the $^{58}Ni + ^{58}Ni$ and $^{64}Ni + ^{64}Ni$ systems exhibited the least sub-barrier fusion. In the present study, we intended to determine whether further increases in sub-barrier fusion occur in $^{74}Ge + ^{74}Ge$ beyond those observed[3] in systems where ^{74}Ge replaced either ^{58}Ni or ^{64}Ni as a collision partner. High precision measurements of cross sections for complete fusion of $^{40}Ca + ^{40,44,48}Ca$ and ^{81}Br, $^{90}Zr + ^{90,94}Zr$, ^{96}Mo have been carried out as well. Those data will be reported on in detail elsewhere.

In the experiments 218–305 MeV, ^{74}Ge beams provided by the Brookhaven National Laboratory (BNL) Tandem Van de Graaff Facility were used to bombard ^{74}Ge targets. Differential cross sections for evaporation residue formation were measured using the MIT-BNL velocity selector (RMS) together with a ΔE-E counter telescope. Calibration details pertaining to the present experiment which have not been previously[2,3] discussed are presented in Sec. II. The evaporation residue measurements span the energy range from 0.90 to 1.24 times the fusion barrier. The evaporation residue cross sections equal the complete fusion cross sections except at the highest energies, where non-negligible fission contributions are expected. Differential cross sections for evaporation residue formation are presented in Sec. III A, and cross sections for complete fusion are presented in Sec. III B together with comparisons to our earlier data for Ni-Ni and Ni-Ge.

We attempt to systematize a number of observations concerning near- and sub-barrier fusion data in Sec. IV. We discuss dynamic processes which may take place during weak-to-strong contact of the collision partners and relationships of fusion to other reaction channels. We summarize our work in Sec. V.

II. EXPERIMENTAL METHOD AND EFFICIENCY MEASUREMENTS

Both source and targets were fabricated from reduced ^{74}Ge powder isotopically enriched to 98.9% (0.15% ^{76}Ge). Targets were 90 to 110 $\mu g/cm^2$ thick on the 8 to 12 $\mu g/cm^2$ formvar and/or carbon backings. A 20 $\mu g/cm^2$ carbon foil, placed some 10 cm behind the target, served to ensure that the charge distribution of the recoiling evaporation residues was equilibrated.

The detection system consisted of a pair of target chamber silicon surface barrier detectors, the RMS, and a ΔE-E counter telescope. The target chamber detectors were placed at angles of 21.8° with respect to the beam axis and subtended solid angles for 0.0405 msr. The elastic scattering yield in these detectors was used for cross section normalization and beam composition monitoring. The RMS—an electrostatic beam separator plus velocity ($E \times B$) filter, and fore and aft magnetic quadrupole doublets—enabled the detection of forward-recoiling evaporation residues to 0° and elimination of contaminant reaction products. The ΔE-E telescope consisted of a ΔE section which contained isobutane at 20 mm Hg and an E section which was a 450 mm^2 silicon surface barrier detector, mounted at the rear of the telescope. The entrance aperture was covered with polypropelene stretched to a

thickness of 70 $\mu g/cm^2$, and the telescope was placed at the image of the aft quadrupole doublet of the RMS.

Two pairs of milled carbon slits were placed into position along the beam axis approximately 1 cm in front of the target assembly. These slits restricted the maximum size of the beam spot on a target to 1.5 mm vertical by 2.5 mm horizontal. Additional focusing was achieved by balancing and minimizing the current from these slits; this current was monitored during the measurements. By this procedure, variations in beam quality and amount of transmitted beam tail were minimized.

The influence of remaining variations in beam tuning upon reproducibility of results was investigated in a series of calibration measurements. In the measurements, ^{127}I ions were elastically scattered from Au targets. The detection system was placed at the same scattering angles on the target chamber's solid-state detectors so that the telescope to monitor yield ratio equalled the corresponding solid angle ratio. The results, including those from Refs. 2 and 3, are displayed as effective solid angles for the detection system in Fig. 1. From the agreement between various sets of measurements we see that the yields are reproducible to within a few percent. We also find that the solid angle monotonically increases from about 1.0 msr at 80 MeV to approximately 1.3 msr at 110 MeV.

To obtain efficiencies appropriate for any given recoiling ion and assign meaningful errors to these quantities, we expanded the investigation of the response of the detection system to the ionic charge from that reported in Ref. 2. Model calculations were performed in which a charge state versus a velocity map of efficiencies was folded with ionic charge state and velocity distributions to give relative efficiencies which could be compared to measured yields. The charge state versus velocity map represented results of detailed ray tracing calculations of effective solid angles. The principal feature of the q-v map was a gradually decreasing effective solid angle for charge states progressively further below the central value coupled to a rapidly decreasing effective solid angle for charge states progressively greater than the central value. The ionic charge-state distribution was taken to have a Gaussian shape with mean value and width as determined from measurements[4,5] of ^{127}I equilibrium charge-state distributions. In Fig. 1, the straight line represents the expected variation in solid angle.

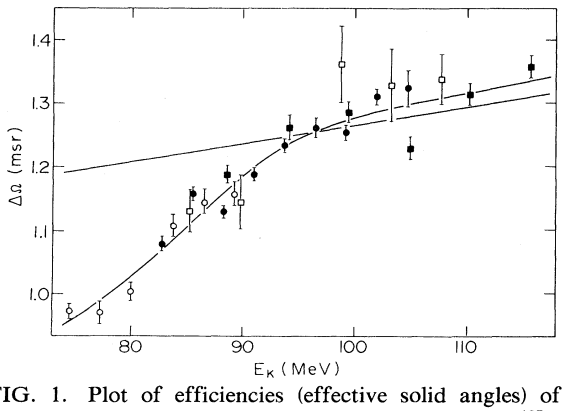

FIG. 1. Plot of efficiencies (effective solid angles) of the detection system determined by elastically scattering ^{127}I ions from Au target. The ordinate gives the yield in the ΔE-E telescope relative to that in the target chamber monitors; the abscissa denotes the kinetic energy of the recoiling ^{127}I ions. The straight solid line represents the prediction based upon the empirical expression (Ref. 6), while the curved line gives the efficiencies calculated using experimental (Refs. 4 and 5) mean charge states.

In the elastic scattering measurements, an empirical expression for the mean charge state $\bar{q}$ of Nikolaev and Dmitriev[6] was employed. In general, this expression tends to underestimate $\bar{q}$ by one or two units at low ion energies and tends to overestimate $\bar{q}$ at high ion energies.[7] For ^{127}I, the empirical expression and experimentally determined $\bar{q}$ are in agreement over the upper portion of the energy range spanned by the data shown in Fig. 1. The steep dropoff of the data from the calculated efficiencies in the 80—100 MeV range is a consequence of the mean charge state crossing the N-M atomic shell closure. Calculations were performed which took into account the rapidly increasing underestimate of $\bar{q}$ by the empirical formula in this energy range. These results follow the data, as can be seen in Fig. 1.

In the vicinity of maximum yield, variations of up to about 5% result from small errors in mean charge-state identification. However, as we have just seen, larger errors are likely to arise if $\bar{q}$ is substantially underestimated. For heavy systems, such underestimates can occur as a consequence of internal conversion processes.[8] To avoid this from happening, an equilibration foil must be placed downstream from the target. To illustrate this point, we present in Fig. 2 results of measurements of relative yields for $^{74}Ge + {}^{74}Ge \rightarrow {}^{148}Gd^*$ evaporation residues taken with as well as without an equilibration foil. Here we find yields peaked at the expected value for q, when a 20 $\mu g/cm^2$ foil was used, and yields peaked some five units higher in q, when the foil was omitted. The shift towards higher q has been enhanced, most likely, by Auger processes.[8] These have been shown[9] to lead to large increases in the mean ionic charge of heavy fission fragments. Finally, we note that the foil resets the equilibrium charge-state distribution except, perhaps, for those recoiling ions caught in a yrast trap. Upon comparison of the distribution of evaporation residues produced in our experiments with the distribution of nuclides known to possess yrast traps,[10] we concluded that the loss of cross section by this means was negligible.

To summarize, errors of on the order of 3—4 % were expected from residual variations in beam tuning. Errors of about 5% were expected from uncertainties in mean charge-state identification. To keep these latter uncertainties minimal, care was taken to avoid substantial underestimates of $\bar{q}$. This was accomplished by being aware of systematic departures of $\bar{q}$ estimated by empirical relations such as that of Ref. 6 from actual values, and, for heavy systems, through the use of an equilibration foil to avoid shifts in $\bar{q}$ resulting from internal conversion.

III. EVAPORATION RESIDUE MEASUREMENTS

A. Differential cross sections

Angular distributions of the evaporation residues, measured in $\frac{1}{2}°$ or 1° steps, are displayed in Fig. 3. Left/right

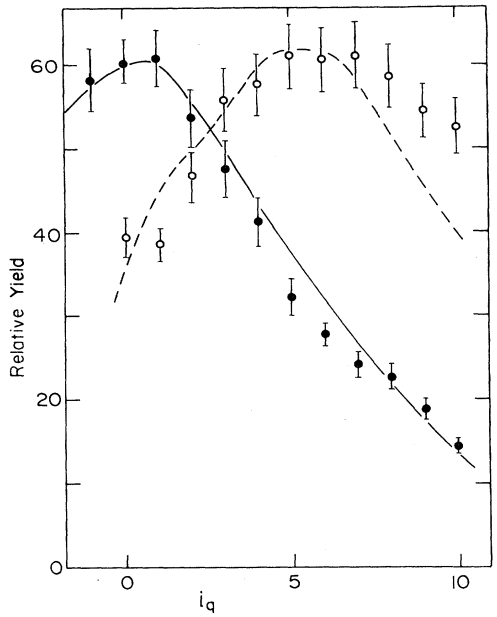

FIG. 2. Plot of the relative yield of $^{74}Ge + ^{74}Ge \rightarrow ^{148}Gd^*$ evaporation residues at $E_{lab}(^{74}Ge)=270$ MeV, $\theta_{lab}=0°$. The abscissa gives the charge state setting of the system relative to the mean value $\bar{q}=29$ predicted by the empirical expression (Ref. 6). Filled circles denote the results obtained using an equilibration foil; open circles represent the results obtained without the foil. The solid curve gives the calculated relative yield; the dashed curve denotes the yield predicted assuming that 30% of the ions have a mean charge state six units higher than expected.

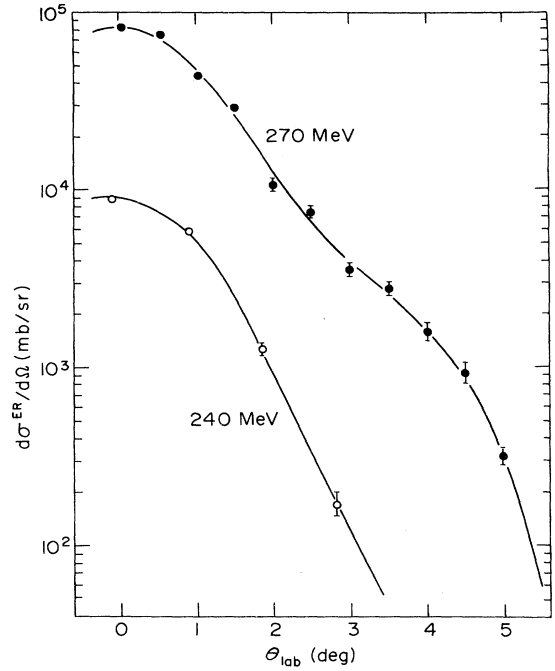

FIG. 3. Angular distributions of the evaporation residues at two representative bombarding energies. Solid lines denote the smoothed angular distributions used for integration purposes.

measurements were performed for each angular distribution to define the true beam axis, and weighted angles were used to take into account the yield dropoff within the 1.3 msr solid angle. The angular distributions are characteristically sharply peaked at 0° with a slight modulation near 3° produced by the transition from predominately neutron evaporation to alpha particle evaporation.[3]

Differential cross sections for Rutherford scattering were used[1-3] to normalize yields: The angular acceptance (taking into account the beam-spot size) of the monitors served to average over the Mott oscillations for these heavy systems. The differential cross sections comprising the angular distributions were integrated over the recoil kinetic energy spectra as were the zero-degree differential cross sections listed in the third column of Table I. The zero-degree data were taken in 5 MeV (lab) steps at the higher bombarding energies and in smaller steps at the lower bombarding energies. These data were converted to cross sections for evaporation residue formation using the smoothly varying results of the angular distribution integrations.

The conversion of evaporation residue yield to cross section was performed using results of the efficiency calculations discussed in Sec. II. We obtained an 8% error from combining in quadrature uncertainties due to beam tuning, mean charge-state identification, and differential cross section integrations. We therefore assigned minimum total errors to the absolute cross sections of 10%.

B. Complete fusion

The cross sections for evaporation residue formation are listed in the fourth column of Table I, and are displayed in Fig. 4. The total errors are given in the fifth column, and are represented by the error bars in Fig. 4. For comparison, statistical errors in the zero degree differential cross sections are given in the third column. The cross sections increase uniformly over the entire measured range from 218 to 305 MeV. The cross sections at the highest energies can be compared to the cross section for evaporation residue formation for the $^{86}Kr + ^{65}Cu \rightarrow ^{151}Tb^*$ system[11] at $E_{lab}(^{86}Kr)=366$ MeV. The compound nuclei are similar and in both instances the center-of-mass energy is some 20% above that of the nominal Coulomb barrier. For $^{74}Ge + ^{74}Ge$, we find that $\sigma^{ER}=435\pm50$ mb; for $^{86}Kr + ^{65}Cu$, the reported value is $\sigma^{ER}=464\pm50$ mb.

Measurements of cross sections for evaporation residue formation and for fission have been performed for the $^{40}Ar + ^{109}Ag \rightarrow ^{149}Tb^*$ (Ref. 12) and $^{35}Cl + ^{116}Sn \rightarrow ^{151}Ho^*$ (Ref. 13) systems. In the sharp cutoff approach, partial waves above about $45\hbar$ were found to give non-negligible fission contributions to complete fusion. To estimate the fission contributions for the slightly less fissile $^{148}Gd^*$ nucleus, we performed multiple-chance fission/particle emission calculations. In these calculations, we used statistical fission parameters determined from simultaneous fits to measured excitation functions and finite range fission barriers.[13,14] For our system, the critical angular momentum, l^{ER}, defined by

TABLE I. Summary of zero-degree differential cross sections and evaporation residue cross sections.

E_{lab} (MeV)	$\bar{E}_{c.m.}$ (MeV)	$\frac{d\sigma^{ER}(0)}{d\Omega}$ (b/sr)	σ^{ER} (mb)	$\Delta\sigma^{ER}$ (%)
305	151.9	113.6 ±5.8	429	12
300	149.4	124.1 ±6.3	444	12
295	146.9	111.3 ±5.7	377	12
290	144.4	98.21 ±5.01	314	12
285	141.9	99.69 ±4.64	301	12
280	139.5	93.21 ±3.64	265	12
275	137.0	81.13 ±3.40	217	12
270	134.5	82.35 ±3.51	206	10
265	132.0	66.04 ±2.86	155	12
260	129.5	54.50 ±2.13	121	12
255	126.9	39.18 ±1.17	82.2	12
250	124.4	33.58 ±1.39	67.1	12
245	122.0	17.50 ±0.51	33.6	12
240	119.5	9.027 ±0.356	16.8	10
235	117.0	3.895 ±0.154	7.18	12
230	114.5	1.433 ±0.073	2.61	12
228	113.5	0.790 ±0.038	1.43	12
226	112.4	0.533 ±0.026	0.960	12
225	111.9	0.311 ±0.022	0.559	12
224	111.4	0.261 ±0.027	0.467	15
223	110.9	0.180 ±0.016	0.321	15
222	110.5	0.125 ±0.013	0.223	15
221	110.0	0.0806±0.0095	0.143	15
220	109.6	0.0507±0.0093	0.090	20
219	109.0	0.0353±0.0059	0.062	20
218	108.5	0.0156±0.0026	0.027	20

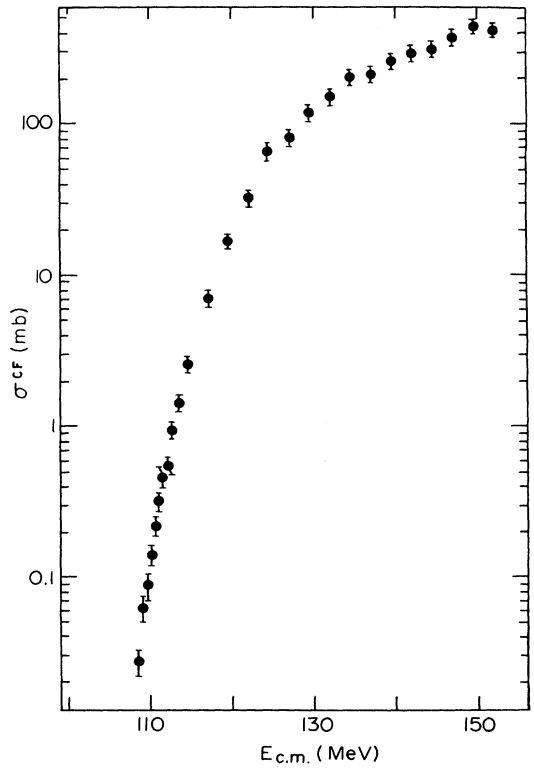

FIG. 4. The excitation function for complete fusion of $^{74}Ge + {}^{74}Ge$ as a function of weighted average center-of-mass energy.

$$\sigma^{ER} = \pi\lambda^2(l^{ER}+1)^2 ,$$

equals $\sim 50\hbar$ for σ^{ER} at 285 and 290 MeV, and equals $\sim 60\hbar$ for σ^{ER} at 305 MeV. The results of the calculations were that we may expect some 2 mb fission at 285 MeV, and, perhaps, 15 mb at 305 MeV.

The reduced excitation function for the $^{74}Ge + {}^{74}Ge$ is compared to the reduced excitation functions for the $^{58}Ni + {}^{58}Ni$, $^{58}Ni + {}^{64}Ni$, $^{64}Ni + {}^{64}Ni$, $^{58}Ni + {}^{74}Ge$, and $^{64}Ni + {}^{74}Ge$ systems in Fig. 5. The scale variables V_0 and R_0 denote the effective fusion barrier height and position, respectively, as obtained by fitting the 30—300 mb portion of the complete fusion excitation function. The fitting was done using the standard expression relating the partial fusion cross sections σ_l to the transmission coefficients T_l, namely,

$$\sigma_l = \pi\lambda^2(2l+1)T_l .$$

The transmission coefficients were calculated numerically using the Wentzel-Kramers-Brillouin (WKB) method, as in Ref. 3, with an inverted harmonic oscillator potential matched to a Coulomb plus centrifugal tail. The effective barrier height extracted from the analysis was 120.8±0.6 MeV, or 4.4 MeV lower than the nominal fusion barrier for spherical nuclei. This nominal barrier height was calculated using the generalized liquid drop potential of Ref. 15, with constants determined in Ref. 16, as part of a global analysis of nuclear masses, elastic scattering, and fission barrier heights. The corresponding difference in barrier heights for the above-mentioned Ni-Ni and Ni-Ge

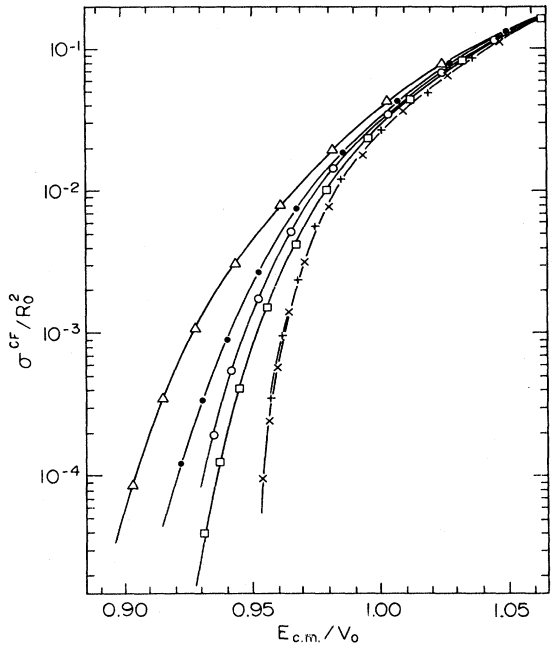

FIG. 5. Reduced excitation functions. Plots of experimental excitation functions scaled using fitted barrier heights and positions. Data for $^{58}Ni+^{58}Ni$ (×) are from Ref. 2; data for $^{58}Ni+^{64}Ni$ (○), $^{64}Ni+^{64}Ni$ (+), $^{58}Ni+^{74}Ge$ (●), and $^{64}Ni+^{74}Ge$ (□), are from Ref. 3; and data for $^{74}Ge+^{74}Ge$ (△) are from the present work. Scale variables for $^{74}Ge+^{74}Ge$ are $V_0=120.8$ MeV and $R_0=8.20$ fm. Those for the other systems are listed in Table IV of Ref. 3.

systems are 4.2, 4.9, 5.2, 5.5, and 6.0 MeV.

From Fig. 5 we see that the $^{74}Ge+^{74}Ge$ cross sections decrease gradually down to far sub-barrier energies, reaching the 30 μb level 17 MeV (c.m.) below the nominal barrier. The gradual decrease in magnitude extends much further below the barrier than that for the symmetric $^{58}Ni+^{58}Ni$ and $^{64}Ni+^{64}Ni$ systems. We also see that further increases in sub-barrier fusion have occurred in the $^{74}Ge+^{74}Ge$ system beyond those found[3] in systems where ^{74}Ge replaced either ^{58}Ni or ^{64}Ni as a collision partner. The pronounced differences in magnitude and slope of the excitation functions for complete fusion at sub-barrier energies cannot be ascribed to variations in height and position of the effective fusion barriers, nor to target-projectile symmetry considerations.

IV. DISCUSSION

We begin our discussion by observing that the standard fusion models increasingly underpredict the cross sections for complete fusion at sub-barrier energies as the systems become more massive. We further note that the s-wave barrier positions, extracted from fits to the above-barrier portion of fusion excitation functions, cease to increase once the systems become heavier than, say, $^{40}Ca+^{40}Ca$. Instead, they level off at values in the range 9.0—9.7 fm when fitting data above 100 mb, and in the range 8.0—8.6 fm when fitting data above 30 mb. The radius constants

$$r_0=R_0/(A_T^{1/3}+A_P^{1/3})$$

slowly decline, reaching a value of about 0.98 fm for $^{74}Ge+^{74}Ge$. We observe[3] that the form factors for the nuclear potential which generates such barriers become increasingly unphysical. One interpretation of the declining radius constants is that they reflect a deeper interpenetration needed to overcome the increasing Coulomb repulsion. The approach of these radii to one Fermi and beyond,[17] plus the unphysical form factors, makes this interpretation difficult.

An alternative explanation is that some of the incident flux may not reach the barrier. Then the transmission coefficient T_l may be replaced by $T_l(1-P_l)$ where P_l represents other open channels, and the sharp cutoff approach implicit in standard fusion models no longer holds. For heavy systems this may happen in a particularly dramatic manner.[17–20]

A possible explanation for the complex isotopic variations seen in our data,[1–3] and in the data of Ref. 21, was advanced in Refs. 22 and 23. There, the point was made that fusion is favored in transfer channels which have positive Q values. In such channels, the pulling off (transfer) of nucleon(s) produces an increase in the kinetic energy of relative motion. It was estimated that probabilities for pair transfer of 6% and 10% for the $^{58}Ni+^{64}Ni$ and $^{58}Ni+^{74}Ge$ systems, respectively, may account for the increased fusion seen in those systems relative to the other Ni + Ni and Ni + Ge systems investigated. Most important, the coupling of the entrance channel to transfer and inelastic channels gives rise[23] to increases in fusion below the barrier and to decreases in fusion above the barrier.

In Refs. 23 and 24, both zero-point motion of collective surface vibrations[25,26] and nucleon transfer were incorporated into a barrier penetration model using a coupled-channel approach. Both transfer and inelastic excitation were shown to be capable of driving the sub-barrier fusion process. The increases in fusion associated with ^{74}Ge might then be ascribed to the widespread presence of low-lying collective levels populated by either or both of these processes.

In Fig. 6(b), we plot the overlap in the charge density[27] for two ^{58}Ni nuclei as a function of the distance between centers. We also plot the overlap in single-particle potential, taken to be of a Woods-Saxon form, with constants[28] which reproduce the single-particle spectrum. In Fig. 6(c), we display the pertinent region spanning the outer maximum of two representative interaction potentials. We see that, even at far sub-barrier distances of closest approach, the overlaps are sufficient[29] for transfer of valence nucleons.

We also observe in Fig. 6 that the overlaps are considerable in the vicinity of the inner turning points. At these radial separations, contact is strong and there are many active orbitals. There will also be a number of active orbitals if a nucleus is soft (recall that a nucleus is soft if there are many different combinations of intrinsic orbitals which are nearly degenerate in energy). There is both experimental[30,31] and theoretical[32,33] evidence that nuclei in the mass region spanned by our measurements, particular-

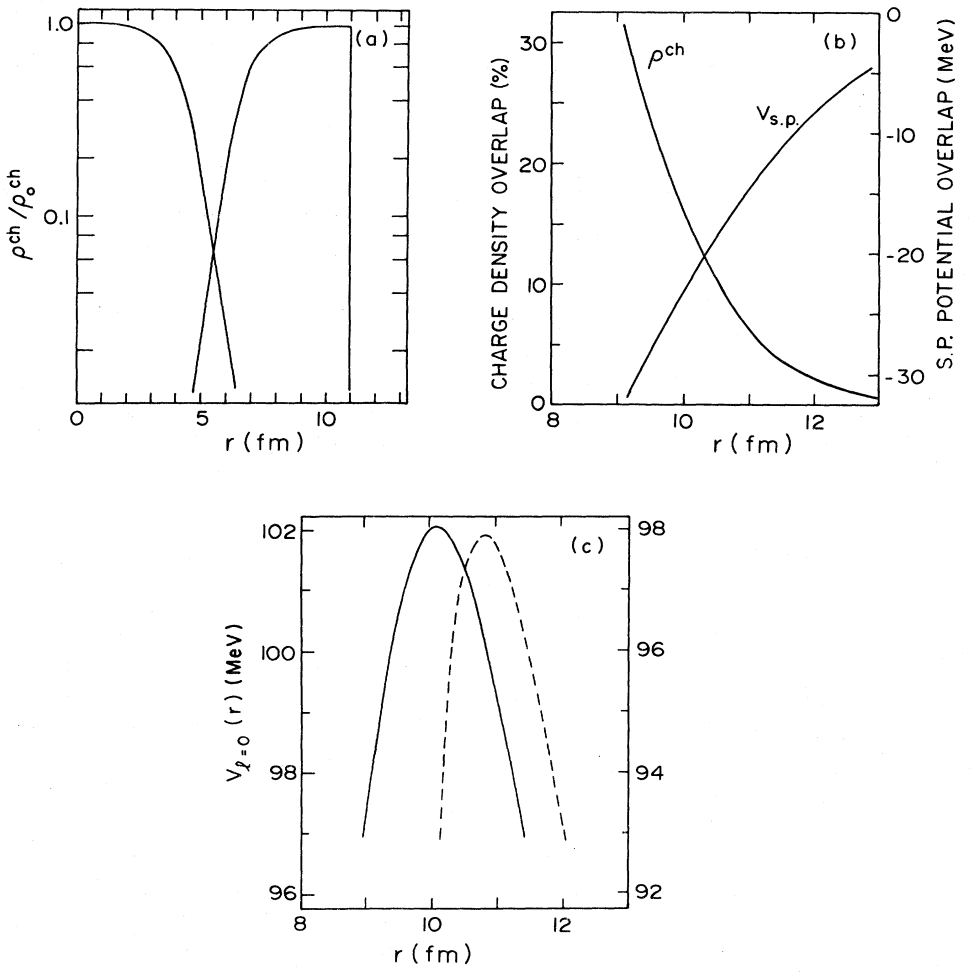

FIG. 6. (a) Plot of the overlap in charge density, determined from electron scattering measurements (Ref. 27), for two ^{58}Ni nuclei whose centers are separated by 11 fm. (b) Plot of the overlaps in charge density and single-particle potential as a function of radial separation between the centers of two ^{58}Ni nuclei. For V_{sp} (Ref. 28), $V_0=49.86$ MeV, $R_0=1.27$ fm, and $a=0.67$ fm. (c) Plots of the outer maximum in the s-wave interaction barrier versus radial separation. The solid curve denotes the barrier maximum calculated using the Krappe-Nix-Sierk potential (Refs. 15 and 16). The dashed curve represents the barrier maximum calculated using the Woods-Saxon potential (Ref. 3).

ly in the vicinity of ^{74}Ge, are soft with respect to shape degrees of freedom. Difficult questions remain on how to incorporate softness properties, how to treat the strong contact stage, and what the interaction potential and effective mass are for fusion.

V. SUMMARY

In this work we measured the excitation function for complete fusion of ^{74}Ge + ^{74}Ge over a broad range in magnitude from 435 mb near 150 MeV down to 27 μb at 108.5 MeV (c.m.). With these experiments we completed the cycle of high precision measurements of excitation functions for complete fusion of ^{58}Ni, ^{64}Ni, and ^{74}Ge with one another from near-barrier to far sub-barrier energies. We found that further increases occurred in the sub-barrier fusion of ^{74}Ge + ^{74}Ge beyond those observed previously in systems where ^{74}Ge replaced either ^{58}No or ^{64}Ni as a collision partner. By constructing reduced excitation functions, we established that the pronounced variations among excitation functions for sub-barrier fusion cannot be ascribed to barrier height and position differences, nor to target-projectile symmetry considerations.

The complex variations in sub-barrier fusion seen in the ^{58}Ni + ^{58}Ni, ^{58}Ni + ^{64}Ni, and ^{64}Ni + ^{64}Ni systems, and in the ^{58}Ni + ^{74}Ge and ^{64}Ni + ^{74}Ge systems, may result from transfer processes serving as doorways for fusion. This inference is drawn from the dinuclear nature of the isotopic variations and from transfer Q-value correlations. A different structural aspect seems responsible for the increases in sub-barrier fusion which occur when either ^{58}Ni or ^{64}Ni is replaced by ^{74}Ge. These increases may be due to softness-related shape changes and/or to the presence of many transfer and inelastic doorways.

ACKNOWLEDGMENTS

The authors wish to acknowledge valuable discussions with Dr. W. Bertozzi, Dr. R. A. Broglia, Dr. D. Cline, Dr. W. S. Freeman, and Dr. J. P. Schiffer. This work was supported by the U.S. Department of Energy under Contract No. DE-AC02-76ER03069.

[1]M. Beckerman, M. Salomaa, A. Sperduto, H. Enge, J. Ball, A. DiRienzo, S. Gazes, Yan Chen, J. D. Molitoris, and Mao Nai-feng, Phys. Rev. Lett. 45, 1472 (1980).

[2]M. Beckerman, J. Ball, H. Enge, M. Salomaa, A. Sperduto, S. Gazes, A. DiRienzo, and J. D. Molitoris, Phys. Rev. C 23, 1581 (1981).

[3]M. Beckerman, M. Salomaa, A. Sperduto, J. D. Molitoris, and A. DiRienzo, Phys. Rev. C 25, 837 (1982).

[4]L. Grodzins, R. Kalish, D. Murnick, R. J. Van de Graaff, F. Chmara, and P. H. Rose, Phys. Lett. 24B, 282 (1967).

[5]S. Datz, C. D. Maok, H. O. Lutz, L. C. Northcliffe, and L. B. Bridwell, At. Data 2, 273 (1971).

[6]V. S. Nikolaev and I. S. Dmitriev, Phys. Lett. 28A, 277 (1968).

[7]H.-D. Betz, Rev. Mod. Phys. 44, 465 (1972).

[8]W. S. Freeman, H. Ernst, D. F. Geesaman, W. Henning, T. J. Humanic, W. Kühn, J. P. Schiffer, B. Zeidman, P. W. Prosser, Phys. Rev. C 28, 919 (1983).

[9]D. Habs, V. Metag, H. J. Specht, and G. Ulfert, Phys. Rev. Lett. 38, 387 (1977); G. Ulfert, D. Habs, V. Metag, and H. J. Specht, Nucl. Instrum. Methods 148, 369 (1978).

[10]J. Pedersen, B. B. Back, F. M. Bernthal, S. Bjørnholm, J. Borggreen, O. Christensen, F. Folkmann, B. Herskind, T. L. Khoo, M. Naiman, F. Pühlhofer, and G. Sletten, Phys. Rev. Lett. 39, 990 (1977).

[11]F. Plasil, R. L. Ferguson, H. C. Britt, B. H. Erkkila, P. D. Goldstone, R. H. Stokes, and H. H. Gutbrod, Phys. Rev. C 18, 2603 (1978).

[12]H. C. Britt, B. H. Erkkila, R. H. Stokes, H. H. Gutbrod, F. Plasil, R. L. Ferguson, and M. Blann, Phys. Rev. C 13, 1483 (1976).

[13]B. Sikora, W. Scobel, M. Beckerman, J. Bislinghoff, and M. Blann, Phys. Rev. C 25, 1446 (1982).

[14]A. J. Sierk, private communication; H. C. Britt, private communication.

[15]H. J. Krappe, J. R. Nix, and A. J. Sierk, Phys. Rev. C 20, 992 (1979).

[16]P. Möller and J. R. Nix, Nucl. Phys. A361, 117 (1981).

[17]M. Beckerman, in Proceedings of the Conference on Nuclear Physics with Heavy Ions, Stony Brook, 1983.

[18]M. Beckerman, M. K. Salomaa, J. Wiggins, and R. Rohe, Phys. Rev. Lett. 50, 471 (1983).

[19]R. Bock, Y. T. Chu, M. Dakowski, A. Gobbi, E. Grosse, A. Olmi, H. Sann, D. Schwalm, U. Lynen, W. Müller, S. Bjørnholm, H. Esbensen, W. Wölfli, and E. Morenzoni, Nucl. Phys. A388, 334 (1982).

[20]W. J. Swiatecki, Nucl. Phys. A376, 275 (1982).

[21]R. Pengo, D. Evers, K. E. G. Löbner, U. Quade, K. Rudolf, S. J. Skorka, and I. Weidl, Nucl. Phys. (in press).

[22]R. A. Broglia, C. H. Dasso, S. Landowne, and A. Winther, Phys. Rev. C 27, 2433 (1983).

[23]R. A. Broglia, in Proceedings of the International Conference on Heavy-Ion Physics and Nuclear Physics, Cantania, 1983.

[24]C. H. Dasso, S. Landowne, and A. Winther, Nucl. Phys. A405, 381 (1983).

[25]H. Esbensen, Nucl. Phys. A352, 147 (1981).

[26]H. Esbensen, A. Winther, R. A. Broglia, and C. H. Dasso, Phys. Rev. Lett. 41, 296 (1978); R. A. Broglia, C. H. Dasso, G. Pollarolo, and A. Winther, *ibid.* 40, 707 (1978); 41, 25 (1978).

[27]J. R. Ficenec, W. P. Trower, J. Heisenberg, and I. Sick, Phys. Lett. 32B, 460 (1970).

[28]A. Bohr and B. R. Mottelson, *Nuclear Structure* (Benjamin, New York, 1969), Vol. 1, p. 239.

[29]J. R. Huizenga, J. R. Birkelund, and W. Johnson, Proceedings of the Symposium on Macroscopic Features of Heavy-Ion Collisions, Argonne, 1976, Argonne National Laboratory Report ANL/PHY-76-2, 1976, p. 1.

[30]J. H. Hamilton, L. H. Crowell, R. L. Robinson, A. V. Ramayya, W. E. Collins, R. M. Ronningen, V. Maruhn-Rezwani, J. A. Maruhn, N. C. Singhal, H. J. Kim, R. O. Sayer, T. Magee, and L. C. Whitlock, Phys. Rev. Lett. 36, 340 (1976); H. P. Hellmeister, U. Kamp, J. Keinonen, K. P. Lieb, R. Rascher, R. Ballini, J. Delaunay, and H. Dumont, Phys. Lett. 85B, 34 (1979); C. J. Lister, B. J. Varley, H. G. Price, and J. W. Olness, Phys. Rev. Lett. 49, 308 (1982).

[31]D. Cline, private communication.

[32]J. W. Negele and G. Rinker, Phys. Rev. C 15, 1499 (1977).

[33]D. Ardouin, R. Tamisier, M. Vergnes, G. Rothard, J. Kalifa, G. Berrier, and B. Grammaticos, Phys. Rev. C 12, 1745 (1975).